Received 31 May 2023; revised 12 September 2023; accepted 12 October 2023.
Date of publication 19 October 2023; date of current version 5 December 2023.

Digital Object Identifier 10.1109/JXCDC.2023.3325706

Modeling and Investigating Total Ionizing Dose Impact on FeFET

MUNAZZA SAYED[1], KAI NI[2] (Member, IEEE), and HUSSAM AMROUCH[1,3] (Member, IEEE)

[1]Semiconductor Test and Reliability (STAR), University of Stuttgart, 70174 Stuttgart, Germany
[2]Department of Microsystems Engineering, Rochester Institute of Technology, Rochester, NY 14623 USA
[3]TUM School of Computation, Information and Technology, Chair of AI Processor Design, Munich Institute of Robotics and Machine Intelligence, Technical University of Munich, 80333 Munich, Germany

CORRESPONDING AUTHOR: M. SAYED (sayedma@iti.uni-stuttgart.de)

ABSTRACT This article presents a novel, simulation-based study of the long-term impact of X-ray irradiation on the ferroelectric field effect transistor (FeFET). The analysis is conducted through accurate multiphysics technology CAD (TCAD) simulations and radiation impact on the two FeFET memory states—high-voltage threshold (HVT) and low-voltage threshold (LVT)—is studied. For both the states, we investigate the deterioration of device characteristics, such as threshold voltage shift (ΔV_{th}) and memory window (MW) degradation, resulting from total ionizing dose (TID) exposure between 10 krad/s and 3 Mrad/s. At a dose rate of 10 krad/s, the FeFET is adequately radiation hardened for both HVT and LVT due to negligible change in MW from the baseline, unradiated case. At a dose rate of 3 Mad/s, an MW degradation of 40% is observed, and the greatest contributor is identified as the HVT state, which shows a 0.5-V increase in ΔV_{th}, compared with 0.08 V ΔV_{th} for LVT at the same dose rate. The difference in radiation responses for HVT and LVT at the same TID is investigated and attributed to the impact of the depolarization electric field (E_{dep}) on the transport of electrons and holes. Consequently, holes form oxide traps that occupy deeper energy levels for HVT compared with LVT, which underlies the V_{th} shift and MW degradation. The resultant I_d–V_g characteristics are in good agreement with the experimental data. Our analysis highlights that the HVT state is sensitive to TID relative to LVT.

INDEX TERMS Emerging memory, ferroelectric field-effect transistor (FeFET), radiation, reliability, total ionizing dose (TID), X-ray.

I. INTRODUCTION

Ferroelectric field-effect transistors (FeFETs) have gained recent acclaim as an emerging memory technology that boasts stellar energy efficiency and nondestructive readout [1]. Since HfO_2 is considered a state-of-the-art gate insulator for all high-κ metal gate technologies [2], HfO_2-based FeFETs offer considerable CMOS compatibility and scalability [3]. Furthermore, this next-generation memory device owes its nonvolatile characteristics to two states of remanent polarization—high-voltage threshold (HVT) and low-voltage threshold (LVT). These correspond to upward and downward ferroelectric polarizations, storing logic 1 and 0, respectively. Ensuring the reliability of each memory state is quintessential, as it affects the validity of stored information [3].

FeFETs are heralded as the forerunners of a promising future of computing by virtue of efficiently addressing the varied requirements of both the traditional and emerging computing applications [1]. Hence, these transistors are relevant for adaptation across a host of disciplines. The extensive list of sectors that would rely particularly on the radiation hardness of ferroelectrics includes space exploration, avionics, medical-Internet of Things (IoT), and nuclear power, among others [4], [5]. However, the prevalence of high-energy radiation in these sectors becomes a liability since it can add up to semi-permanent or even irreversible ionizing damage over the device lifetime [6]. Given the far-reaching applications of FeFETs in high-radiation environments, the impact of radiation on its memory states is worth explication. This is currently a novel and highly consequential area of research.

Total ionizing dose (TID) refers to the cumulative effects of prolonged radiation exposure. An immediate aftereffect of TID is that the stored information in memory cells may be lost or incorrectly read. This manifests as undesirable

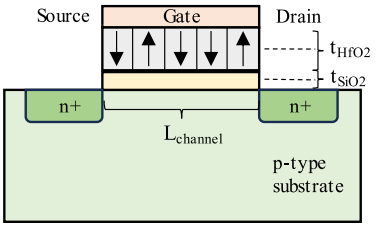

Parameter	Value (nm)
t_{HfO2}	10
t_{SiO2}	0.6
$L_{channel}$	100

FIGURE 1. Unpolarized FeFET (baseline) in the MFIS architecture, as used in TCAD simulations. The corresponding geometrical parameters are also shown.

drifts in device characteristics, such as threshold voltage (V_{th}) and memory window (MW) degradation [7], compromising device functionality. To circumvent the aforementioned concerns, it is essential to perform a thorough analysis of TID impact for both HVT and LVT.

Our Key Contributions: This work is the first-of-its-kind analysis of TID impact on the two FeFET memory states, conducted on Sentuarus technology CAD (TCAD). It is realized through a novel three-step methodology, wherein the HfO_2 layer is: 1) polarized, corresponding to HVT and LVT states; 2) irradiated by X-ray dose rates between 10 krad/s and 3 Mrad/s, and finally; and 3) occupied with holes at respective trap activation energies for HVT and LVT. The final step results in the I_d–V_g characteristics that capture the effects of radiation through V_{th} shift (ΔV_{th}) and MW degradation. For the range of dose rates considered, it is observed that ΔV_{th} increases progressively for HVT, and only marginally for LVT, leading to considerable MW degradation at 3 Mrad/s. This affirms the radiation hardness of the LVT state compared with HVT. The results—in good agreement with the experimental data—are attributed to the difference in the depolarizing electric field distributions of HVT and LVT, which dictates trap occupation at either: 1) deeper energy levels, i.e., toward the interface for HVT or 2) shallow levels, i.e., toward the electrodes, for LVT. We account for the charge distribution with respect to energy levels in this analysis.

II. RELATED WORKS

The radiation hardness of ferroelectrics is well-established in literature [8]. Chen et al. [9] first experimentally reported the impact of gamma ray irradiation on the performance of the HZO-based FeFET memory across a ten-year extrapolated period. It was concluded that remanent polarization decreases due to radiation-induced vacancies and lattice distortion. Previously, Yan et al. [10] developed a theoretical model to analyze the electrical characteristics of a p-channel metal ferroelectric insulator semiconductor (MFIS) structure, concluding that the device is strongly affected by incident radiation of 200 krad/s that can potentially compromise its reliability. However, none of these works accounted for TID impact on the memory states.

Dai et al. [3] in a timely and robust experimental analysis, considered TID impact on the HZO transistor. This work accesses the I_d–V_g transfer characteristics and uses the ΔV_{th} parameter to determine radiation damage for both the HVT and LVT cases, irradiated to 1 Mrad/s. Considering oxide and interface traps, in addition to polarization switching, as possible sources of memory state degradation, this article concluded that oxide traps are the single greatest contributors to the ΔV_{th} shift, albeit manifested differently for the two states. Finally, the study affirmed the robust TID tolerance of FeFETs. Furthermore, Trump [12] more recently conducted a comprehensive and rigorous TID analysis in both the n-type and p-type FeFETs, specifically for the case of X-rays. They observed greater radiation induced HVT deterioration, compared with LVT, and attributed this to the impact of the depolarization field. Nonetheless, the lack of a simulation-based study in this area necessitates a device-level analysis, as detailed in this article.

III. UNDERLYING MECHANISM OF RADIATION

X-ray radiation is an example of high-energy electromagnetic radiation that loses most of its energy by the ionization of target atoms [8], resulting in electron–hole (e/h) pair generation. The amount of energy deposited per unit mass of a material at the point of incidence is called dose or total dose [12]. The effect of TID radiation is most pronounced in the oxide layer. The rate of e/h pair generation is a material-dependent process that is further influenced by the type and energy of incident particles. This phenomenon is known to change the electrical properties of materials at dose rates as low at 1 krad/s [8]. Furthermore, X-ray radiation is considered to be one of the most effective types of radiation, known to generate a high number of unrecombined holes [12].

Following generation, a fraction of the e/h pairs are annihilated by prompt recombination. The remaining unrecombined holes are *trapped* within the oxide layers, owing to their higher mass and lower mobility. Insulators such as HfO_2 and SiO_2 are characterized by wide bandgaps and hole mobility several orders of magnitude lower than that of electrons [12]. This accounts for the slower hopping transport mechanisms that cause holes to move toward the HfO_2–SiO_2 interfacial layer [13] upon breaking chemical bonds and releasing H^+ ions. Conversely, electrons are extremely mobile and can be swiftly swept out toward the electrode due to TID impact or even weak electric fields.

The remaining holes occupy traps at various energy levels. Oxygen vacancies and interstitial atoms are considered to be the main culprits behind trap creation in ferroelectrics [14]. The extent of radiation-induced degradation depends highly on device process and structure [15], leading to either oxide or interface trap occupation. This analysis focuses exclusively on the oxide trap component, as interface traps are assumed to have a relatively small contribution to ΔV_{th}. This is because the subthreshold swing, which is characterized by interface trap states, was experimentally found to be negligible between HVT and LVT following TID radiation [3]. Another point of consideration that dictates the concentration of oxide traps is the extent of scaling of gate oxide, such that total charge accumulation is directly proportional to oxide thickness [16]. However, for oxides thinner than 10 nm, trapped charges at the interface are

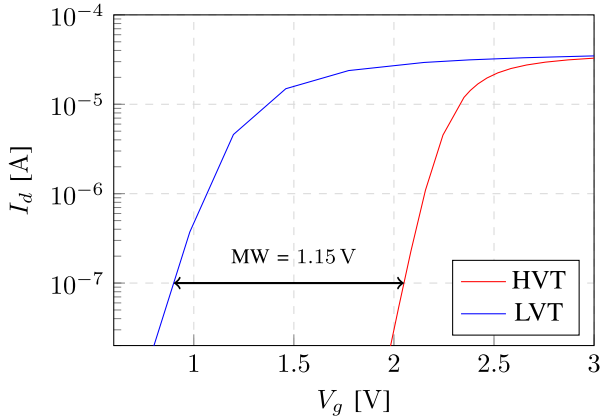

FIGURE 2. **Large MW of 1.15 V exists between the baseline HVT and LVT, obtained as the difference in V_{th} at I_d of 10^{-7} A. The memory states are attained by providing gate voltage pulse of −4 V for HVT and 4 V for LVT.**

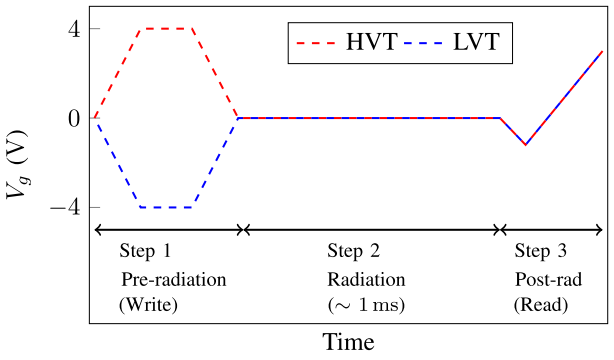

FIGURE 3. **Simulation methodology can be characterized into three steps, shown here with respect to the gate voltage pulse for both HVT and LVT (not drawn to scale). During Step 2, the device is subject to X-ray radiation in excess of 10 krad/s, given that X-rays are known to best capture TID impact compared with other types of radiation. Step 1 prepares the device for radiation and accounts for polarization; Step 3 gives the I_d–V_g characteristics that are used to access TID impact on the memory states. The steps are executed in succession through transient simulations.**

TABLE 1. **TCAD input parameters.**

Parameter	Description	Value	Unit
μ_e	Electron mobility	20	$\mathrm{cm\,V^{-1}\,s^{-1}}$
μ_h	Hole mobility	10^{-5}	$\mathrm{cm\,V^{-1}\,s^{-1}}$
χ_e	Electron affinity	2.5	eV
	Bandgap	5.6	eV

neutralized by annealing attributed to tunneling processes i.e., restoration of bonds to unoccupied oxygen vacancies [12]. This mechanism leaves no net oxide positive charge, due to the joining of tunneling fronts at the oxide center [16]. Furthermore, the thinner the oxide, the fewer the availability of trapping sites for charges [17]. Another aspect is that the thinner the oxide, the larger the capacitance and lesser the shift. Oxides such as the 0.6-nm SiO_2 in this analysis are unaffected by TID.

Moreover, the depth of oxide charge trapping is a phenomenon that differs between HVT and LVT due to differences in the depolarization field (E_{dep}). In the case of HVT, electrons move against the direction of E_{dep} and are expelled from the metal electrode, whereas heavier holes occupy deeper traps toward the interface. In the case of LVT, electrons move against the direction of E_{dep} but toward the interface, while holes move toward the electrodes. Hence, the subsequent-radiation induced trap occupation causes negative shift of V_{th}, which increases for HVT, compared with LVT, with increasing dose rate.

IV. SIMULATION METHODOLOGY

This section models TID impact due to X-rays for a 2-D n-type FeFET, as shown in Fig. 1. Furthermore, Fig. 2 shows the corresponding large MW of 1.15 V, given by the threshold voltage (V_{th}) difference at a drain current of 10^{-7} A. TID modeling consists of the steps of e/h pair generation, initial recombination, and oxide trap occupation for the two polarization states. A TCAD analysis is presented in three steps to account for the underlying physics processes. The stepwise breakdown of the entire analysis is shown in Fig. 3 with respect to the gate voltage (V_g) pulse across time.

Step 1 (Preradiation): In this section, 1) the device is readied for the next step of radiation and 2) HVT and LVT states are programmed.

1) The material definition of HfO_2 is changed from the default of insulators to semiconductor oxides in TCAD (through the "OxideAsSemiconductor" material definition). The values of important parameters are taken from literature [18], [19] and summarized in Table 1. All other material parameters are the same as the default insulator definition. The physical models include the doping-dependent model, effective intrinsic density model, and high-field saturation model for mobility.
2) The two polarization states are ascribed to a difference in the V_g pulse, such that a negative and positive pulses denote HVT and LVT, respectively, as shown in Fig. 3. Polarization is added to the modified HfO_2 layer by activating the Preisach model, which simulates multidomain polarization switching [20].

Step 2 (Radiation): The TCAD gamma radiation model is invoked in a transient simulation to obtain the effects of X-ray irradiation in the HfO_2 layer. Radiation dose rates between 10 krad/s and 3 Mrad/s are investigated, since FeFET radiation hardness is established in literature at lower doses [3]. The subsequent e/h pair generation parameter (G_r) depends on the electric field (F) [21]. Mathematically, it can be described as [21]

$$G_r = g_0 \cdot \frac{dD}{dt} \cdot Y(F) \tag{1}$$

$$Y(F) = \left(\frac{F + E_0}{F + E_1}\right)^m \tag{2}$$

where D is the dose (rad), dD/dt is the dose rate (rad/s), g_0 is the rate of generation of e/h pairs ($\mathrm{rad^{-1}\,cm^{-3}}$), and E_0,

TABLE 2. TCAD input parameters: radiation model.

Parameter	Description	Value	Unit
g_0	Rate of e/h pair generation	7.6×10^{12}	$\mathrm{rad}^{-1}\,\mathrm{cm}^{-3}$
E_0	Fitting parameter	0.1	$\mathrm{V\,cm}^{-1}$
E_1	Fitting parameter	1.35	$\mathrm{V\,cm}^{-1}$
m	Fitting parameter	0.9	-

E_1, and m are the fitting parameters, shown in Table 2; g_0 is a material-dependent parameter, conventionally calculated in literature for SiO_2 [13]. It depends on the material density (ρ) and the energy required to produce an e/h pair ($E_{e/h}$). In this analysis, g_0 for HfO_2 is given by

$$g_0 = \frac{\rho \times 6.24 \times 10^{13}}{E_{e/h}} = 3.5 \times 10^{13} \tag{3}$$

where ρ is 9.68 $\mathrm{g\,cm}^{-3}$, 1 rad/s is 6.24×10^{13} $\mathrm{eV\,g}^{-1}$ [22], and $E_{e/h}$ is 16.8 eV, assumed to be 3 × HfO_2 bandgap [23].

The fitting parameter values in (2) are taken from literature [24] for the specific case of X-ray irradiation. Here, $Y(F)$ is the yield function that gives the fraction of holes that survive initial recombination. Recombination rate is a picosecond process, which depends on the type and energy of incident radiation, in addition to material properties [8]. To account for recombination at deeper defect levels, the Shockley–Reed–Hall model is used.

Thus, the input parameters for our analysis are g_0, $Y(F)$, and dose rate. The dose rate is ramped up, from 0 to x rad/s, within 1 ms, to optimize for simulation speed. This ramping is in accordance to the simulation framework of [22].

Step 3 (Postradiation): In this step, the I_d–V_g transfer characteristics at different radiation dose rates are extracted, given the following inputs to TCAD: 1) concentration of surviving holes, as output from Step 2 and 2) occupation of holes as per dose rate-dependent trap activation energies in the HfO_2 layer.

1) Step 2 outputs the "radiation generation" parameter G_r ($\mathrm{cm}^3\,\mathrm{s}^{-1}$). This gives the concentration of the remaining holes that are considered to be the fixed charges trapped in the oxide (N_{OT}), assuming that electrons are expelled [13]. Hole concentration is defined through the bulk trap definition of charges and given as "donor" traps in the HfO_2 layer. The electron and hole cross sections are 6.8×10^{-14} and 5×10^{-14} cm^2, respectively [18]. From [13]

$$N_{OT} = g_0 \cdot D \cdot Y(F). \tag{4}$$

The concentration of N_{OT} depends on oxide type, electric field, and incident particle energy [18]. Oxide trap concentration with respect to radiation is shown in Fig. 4 for HVT and LVT, and is of the order of 10^{16} cm^{-3} at the highest dose rate of 3 Mrad/s. As evident for both the polarizations, N_{OT} concentration increases with increasing radiation dose rate.

2) Hole occupation is determined by defining the trap activation energy (E_t), which is the energy of the center of the trap distribution. This is a user-defined parameter that is changed with respect to radiation dose rate through the E_{mid} value. Given HfO_2 bandgap of 5.6 eV, E_t is specified with respect to the valence band [22], with progressively increasing energy levels corresponding to higher dose rates. This is evident in the HVT case, as shown in Fig. 5. For LVT, E_t is fixed, as will be reasoned in Section V. Mathematically

$$E_t = E_{mid} + E_v + E_{shift} \tag{5}$$

where E_v is the valence band energy, and E_{shift} is a shifting parameter (0 by default).

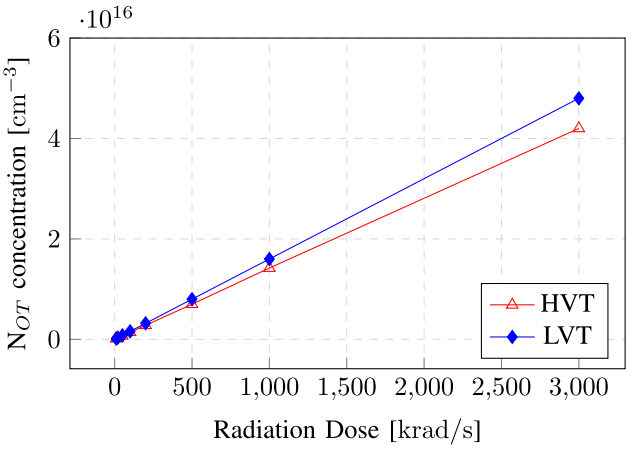

FIGURE 4. Concentration of oxide traps (N_{OT}) for HfO_2 increases linearly with radiation dose rate for both HVT and LVT. This is because N_{OT} is directly proportional to dose rate D and the rate of generation of e/h pairs g_0, the latter being a material-dependent property.

The relationship between E_t and dose rate is as follows. Both these parameters are simultaneously changed to best fit the I_d–V_g curves obtained from the experimental measurements [11]. There is one particular E_t value corresponding to each dose rate. First, each dose rate gives an N_{OT} value, and second, E_t is changed by carefully calibrating TCAD to fit the experimental data of the n-type FeFET subject to X-ray irradiation [11]. In HfO_2, E_t is calibrated by first considering the relationship between E_t and hole concentration in SiO_2 [25]. The conclusion from literature is that the hole occupational probability increases as E_{mid} increases, since the hole emission factor decreases at higher E_{mid} [25]. Indeed, the same trend holds for HfO_2 and has been implemented in our analysis. Subsequently, values of E_t and N_{OT} are entered as inputs to the TCAD trap model. For the HVT case, the closest fit to experimental data was obtained at $E_v + 0.3 \leq E_t \leq E_v + 1.2$ eV and $1.4 \times 10^{14} \leq N_{OT} \leq 4.2 \times 10^{16}$ cm^{-3}; for the LVT case, the fit was obtained at $E_v + 0.3$ eV and $1.5 \times 10^{14} \leq N_{OT} \leq 4.8 \times 10^{16}$ cm^{-3}, both the cases ranging for 10 krad/s– 3 Mrad/s dose rate.

The traps are defined in TCAD through the "level" distribution, for which the corresponding concentration of charge distribution is volumetric, given in cm^{-3}. Trapped

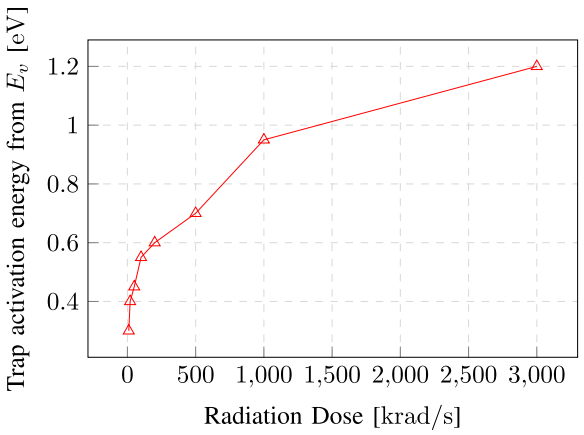

FIGURE 5. **Trap activation energy is a user-defined parameter that is increased with radiation dose rate for HVT, by changing the value of E_{mid} (0.3–1.2 eV) with respect to the valence band energy E_v. At lower dose rates up to 100 krad/s, the fraction of holes that survive initial recombination i.e., hole yield, eventually occupies energy traps closer to the HfO_2 valence band. Hence, activation energy is low at these dose rates. At higher dose rates, the fractional yield increases and holes are captured at relatively deeper trap levels, i.e., closer to the oxide interface. This is accounted for by the higher trap activation energy at higher dose rates.**

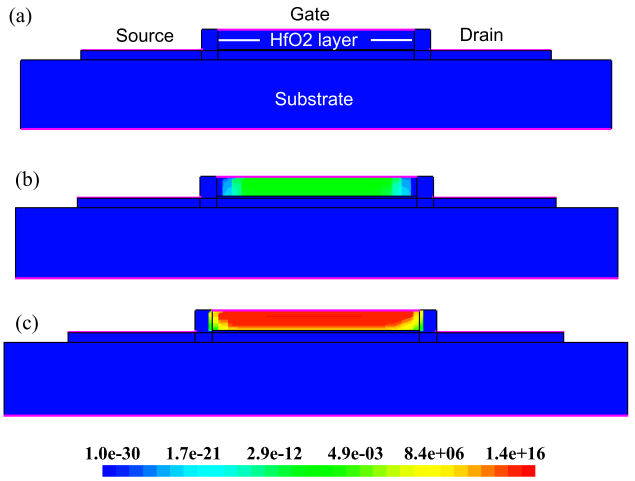

FIGURE 6. **Distribution of trapped holes (cm^{-3}) for the HVT case (a) before subjecting the HfO_2 layer to TID and (b) after TID of 10 krad/s (c) 1 Mrad/s. For (b), trapped hole concentration $N_{OT} = 1.4 \times 10^{14}$ cm^{-3} and activation energy $E_t = E_v + 0.3$ eV. For (c), $N_{OT} = 1.42 \times 10^{16}$ cm^{-3} and $E_t = E_v + 0.95$ eV. N_{OT} in the oxide region increases corresponding to increasing radiation dose. Here, the effect of E_t on the expression of trapped holes is evident. These parameters result in I_d–V_g plots (Fig. 10 in this analysis) that are calibrated to experiment [11].**

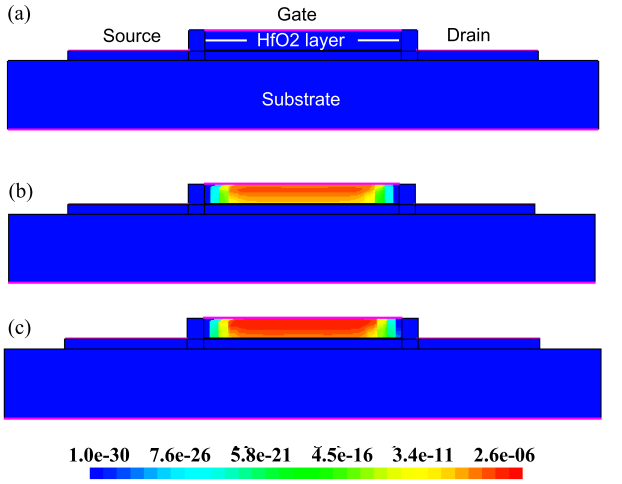

FIGURE 7. **Distribution of trapped holes (cm^{-3}) for the LVT case (a) before subjecting the HfO_2 layer to TID and (b) after TID of 10 krad/s (c) 1 Mrad/s. For (b), trapped hole concentration $N_{OT} = 1.5 \times 10^{14}$ cm^{-3} and activation energy $E_t = E_v + 0.3$ eV. For (c), $N_{OT} = 1.6 \times 10^{16}$ cm^{-3} and $E_t = E_v + 0.3$ eV. N_{OT} in the oxide region increases corresponding to increasing radiation dose. Here, the effect of E_t on the expression of trapped holes is evident. These parameters result in I_d–V_g plots (Fig. 11 in this analysis) that are calibrated to experiment [11].**

holes are relatively stable and immobile, [12] which is ensured in this analysis by the definition of hole traps in the oxide bulk. Hole recovery experiments conducted at zero bias by [11] did not show any recovery, and hence, the holes remain trapped for the entirety of our analysis.

The TID-induced trapped hole (cm^{-3}) profile is shown for HVT (Fig. 6) and LVT (Fig. 7) for the unradiated case and irradiated cases at 10 krad/s and 1 Mrad/s. The plots show the relationship between E_t and N_{OT} at the given dose rates, highlighting the effect of E_t on the trapped charge concentration, which leads to different charge distribution profiles for HVT and LVT.

Finally, we have chosen to focus on the OFF state in our analysis, since, for most memory sensing applications, the FeFET will remain in the OFF state. For instance, in the HVT state, the device is always in the OFF state, even at $V_d \neq 0$, and hence, there is no current flow through the device. A current will only flow when performing a read operation, but this duty cycle is very low. With a small channel current and low V_d, we expect to see no difference in hole trapping mechanisms at the ON state compared with the OFF state.

V. RESULTS AND DISCUSSION

The results highlight the extent of ΔV_{th} due to TID for both HVT and LVT, in conjunction with MW degradation. *Step 1:* With the application of an electric field, polarization varies nonlinearly, exhibiting a hysteresis loop dependency in ferroelectrics [26]. A progressive increase in electric field causes the entire specimen to behave as a single domain, and the ferroelectric exhibits upward or downward pointing polarization states [27] with respect to the channel. This is due to the formation of an inversion channel in the p-substrate layer when the ferroelectric is incorporated in an FET, and V_g is applied [28]. The relationship between the electric field and V_g is that the latter depends on the series capacitance, which in turn influences the electric field in the gate-stack, producing two distinct memory states [3]. However, polarization can be disturbed by the presence of a depolarization field (E_{dep}), which is the built-in electric field

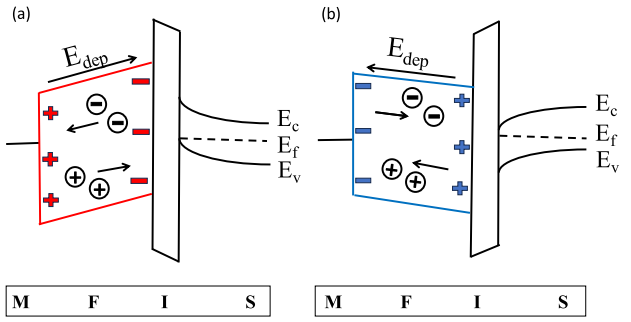

FIGURE 8. Energy band diagrams for (a) HVT and (b) LVT in the MFIS layout. For the HVT case, the depolarization electric field (E_{dep}) causes electron transport in the opposite direction, toward the metal electrode, while holes transport slowly toward the HfO_2-SiO_2 interface. This leads to charge trapping at deeper energy levels. However, due to the difference in electric field, LVT has a different radiation response, characterized by hole accumulation at shallower levels.

caused by polarizing charges in the ferroelectric. E_{dep} plays a substantial role in the transport mechanisms of electrons and holes [11], as elaborated in the next step.

Steps 2 and 3: As a result of TID radiation, the mechanism of charge transport and trapping exhibits notable differences between HVT and LVT, which is evident from the respective energy band diagrams in Fig. 8. In the HVT case, E_{dep} points toward the channel, as shown in Fig. 8(a). Hence, the electrons in the oxide layer (following generation and recombination with holes) are repelled away from the HfO_2–SiO_2 interface, in the opposite direction of the electric field. Consequently, electrons are swiftly removed from the metal electrodes, given the higher electron mobility, and propulsion by drift–diffusion processes.

The bulkier holes end up occupying various trap levels that span energy levels above the HfO_2 valence band. The hole trapping event occurs in conjunction with recombination until equilibrium is achieved. As shown in Fig. 9, a trapping event occurs when an electron occupying an oxide defect is forced into the valence band under an electrostatic potential [22]. This process depends on the trap activation energy and causes the emitted electron to recombine in the valence band, leaving behind a trapped hole in the defect. With increasing dose rates, a greater number of e/h pairs are produced; the unrecombined electrons are driven out, whereas holes are trapped at increasingly deeper sites. Accordingly, the HVT analysis considers the accumulation of holes across trap levels from 0.3 to 1.2 eV above the HfO_2 valence band.

By extension, hole trapping in HfO_2 is the phenomenon responsible for the particular V_{th} shift seen for HVT, given in Fig. 10. It is evident that at 10 krad/s, there is negligible V_{th} shift compared with the baseline, unradiated case, such that the I_d–V_g curves of the two cases overlap almost perfectly. This is testimony to the exceptional radiation hardness of FeFETs at dose rates up to 10 krad/s. At 20 krad/s, there is a slight, negative V_{th} shift, which becomes more pronounced with the progressive increase of radiation dose rate.

In the LVT case, E_{dep} points away from the channel, as shown in Fig. 8(b). Thereby, following recombination,

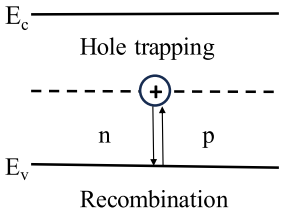

FIGURE 9. Charge trapping depicts the capture of holes in a trapping site above the valence band [22]. This occurs as an electron, previously occupying the trap, is knocked down to the valence band upon loss of energy. The electron then further recombines, leaving behind a hole occupancy in the trap.

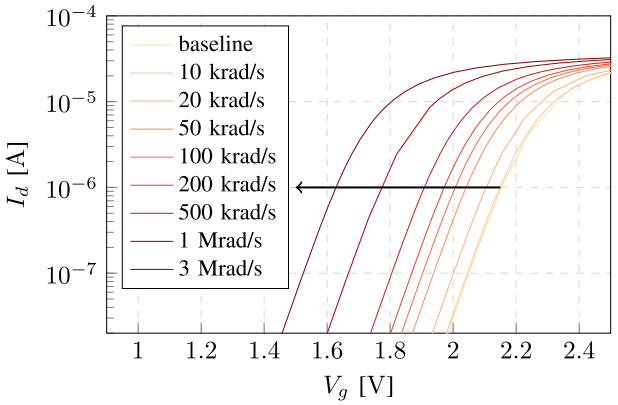

FIGURE 10. Progressive increase in negative shift of V_{th} with radiation dose rate in the HVT case highlights the phenomenon of TID-induced radiation damage. At low dose rate of 10 krad/s, the device is almost unaffected by radiation, which affirms ferroelectric radiation hardness at this dose rate. At 3 Mrad/s, there is a 0.5-V V_{th} shift, indicating worst case scenario.

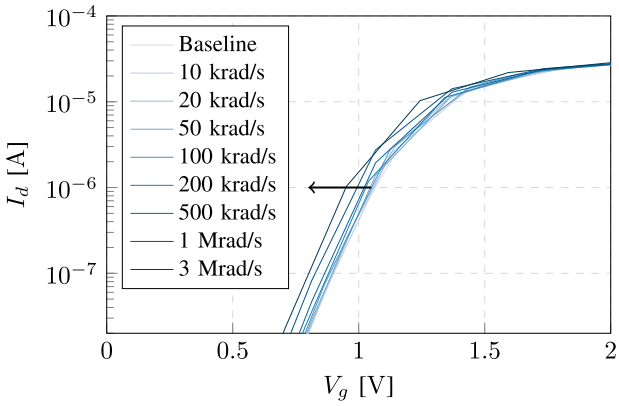

FIGURE 11. Progressive increase in V_{th} with radiation dose rate in the LVT case highlights the phenomenon of minimal TID-induced radiation damage, since the shift in V_{th} is indistinguishable between 10 krad/s and 3 Mrad/s. Hence, this state is conclusively reliable in its radiation response.

electrons move in the opposite direction and begin to collect at the oxide interface, while holes are drawn toward the metal electrodes. The remaining holes occupy shallower energy levels due to the impact of E_{dep} [3], [11], hindering charge build-up. Accordingly, the LVT analysis considers hole accumulation at a shallow trap level of 0.3 eV above the

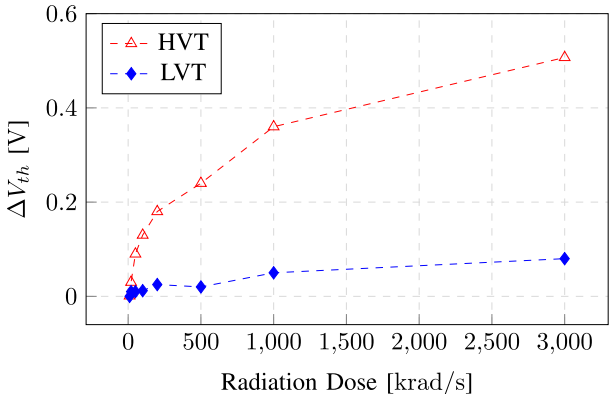

FIGURE 12. Shift of threshold voltage (ΔV_{th}) gives the deviation from the baseline unradiated case, shown here for HVT and LVT. A higher ΔV_{th} is indicative of device deterioration. HVT, having higher ΔV_{th}, is relatively less radiation hardened than LVT.

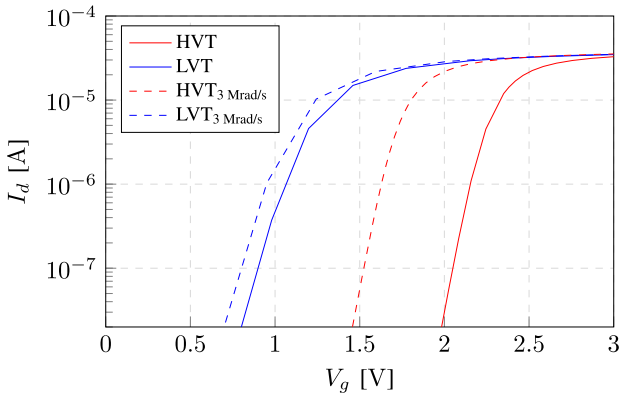

FIGURE 13. Comparison of MW degradation between the states at baseline case (solid) and that of the highest dose rate of 3 Mrad/s (dashed), showing a 40% shrinkage of MW as an aftermath of TID.

TABLE 3. Relative MW comparison to experimental data.

Dose	MW (V) values:	
	This work	Jiang et al.
0 rad	1	1
10 krad	1	1
20 krad	0.93	0.98
50 krad	0.76	0.97
100 krad	0.71	0.81
200 krad	0.69	0.74
500 krad	0.54	0.56
1 Mrad	0.065	0.15
3 Mrad	0	0

HfO_2 valence band, for all the radiation dose rates. It can be seen from Fig. 11 that the V_{th} shift is low, even at a dose rate as high as 3 Mrad/s. The phenomenon responsible for the

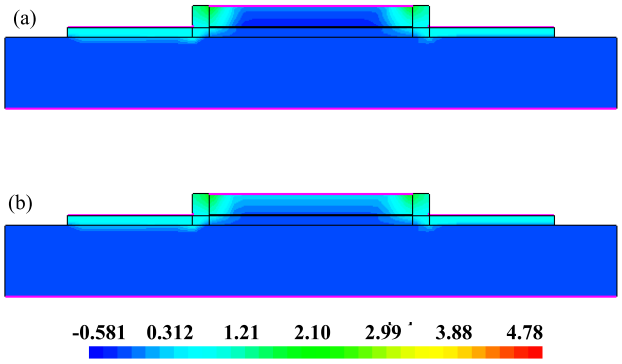

FIGURE 14. Distribution of electrostatic potential (V) for the HVT case (a) before radiation and (b) after 1 Mrad/s shows visible change in potential due to trapped holes. This is expected, considering the V_{th} shift of 0.36 V between cases (a) and (b) (Fig. 12).

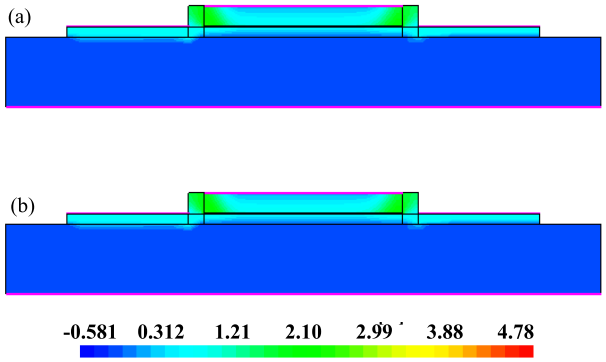

FIGURE 15. Distribution of electrostatic potential (V) for the LVT case (a) before radiation and (b) after 1 Mrad/s, showing the negligible change in potential due to trapped holes. This is expected considering the relatively small V_{th} shift of 0.05 V between (a) and (b), compared with the HVT case at the same dose rate (Fig. 12).

marginal V_{th} shift is the mechanism of hole trapping away from the HfO_2–SiO_2 interface. Fig. 12 shows a comparison of HVT and LVT with respect to the ΔV_{th} metric across a range of dose rates. It can be concluded that the LVT state is more radiation hardened than HVT.

In addition to V_{th}, MW degradation is another compelling metric that clearly indicates radiation-induced device damage and is considered a figure-of-merit for nonvolatile memories [27]. MW degrades with increasing dose rate, showing a 40% shrinkage at the highest dose rate of 3 Mrad/s, as shown in Fig. 13. These trends are in good agreement with the experimental results [11]. A thorough comparison of MW degradation between this analysis and literature is presented in Table 3.

Furthermore, the change in the distribution of electrostatic potential with trapped charge before and after 1 Mrad/s of radiation is evident for HVT (Fig. 14) and LVT (Fig. 15). The results are expected, as per Fig. 12, showing greater V_{th} shift in the HVT case at 1 Mrad/s radiation (0.36 V), compared with LVT. Therefore, a comparison of the electrostatic potential before and after radiation shows more change in the potential for the HVT case compared with the LVT. In the case of the latter, due to the lower V_{th} shift in I_d–V_g between

the unradiated and irradiated case (0.05 V), the potential remains relatively unchanged.

The experimental irradiation [11] is conducted on the 28 nm high-κ metal gate technology, with 10-nm thick HZO layer. The HVT and LVT states are programmed with -4 and 4 V V_g pulse, respectively. The device is then subject to X-ray dose rate of 29 krad(SiO_2)/min, which is incremented in time to reach the desired dose; for example, by 29 krad/min for 0.35 min, equaling a dose of 10 krad. Subsequently, the corresponding I_d–V_g characteristics are obtained at each dose. In other words, while the dose rate remains constant, time is the varying factor. Our analysis establishes an equivalency to the same by varying the dose rate, while keeping the time constant. This is possible since the N_{OT} value remains unchanged even if our analysis is conducted for 1-s dose time (instead of 1 ms).

VI. CONCLUSION

In this work, we presented a novel modeling analysis that captures the effect of TID radiation in the two memory states of an FeFET. This is supplemented by a through explanation of the underlying device physics that results from ionization. The physics-based TCAD analysis considers trap formation at different levels of the ferroelectric, for the HVT and LVT case. It is observed that the HVT state shows greater deterioration than LVT, which is evident from a 40% MW degradation at 3 Mrad/s. We conclude that the difference in radiation response is attributed to the impact of the depolarization field on the direction of transport of electrons and holes. This analysis affirms the relative radiation hardness of the LVT case, compared with HVT, up to a dose rate of 3 Mrad/s.

ACKNOWLEDGMENT

The authors would like to thank Om Prakash, Swetaki Chatterjee, Shivendra Singh Parihar, Simon Thomann, Shubham Kumar, and Florian Klemme from the Chair of Semiconductor Test and Reliability, Stuttgart, Germany, for their valuable support.

REFERENCES

[1] A. I. Khan, A. Keshavarzi, and S. Datta, "The future of ferroelectric field-effect transistor technology," *Nature Electron.*, vol. 3, no. 10, pp. 588–597, Oct. 2020. [Online]. Available: https://www.nature.com/articles/s41928-020-00492-7

[2] (2023). *en-USMajor Differentiation to Competition—Ferroelectric Memory Company*. [Online]. Available: https://ferroelectric-memory.com/technology/major-differentiation-to-competition/

[3] D. Dai et al., "Robustly stable ferroelectric polarization states enable long-term nonvolatile storage against radiation in HfO_2-based ferroelectric field-effect transistors," *ACS Appl. Mater. Interfaces*, vol. 14, pp. 51459–51467, Nov. 2022. [Online]. Available: https://pubs.acs.org/doi/full/10.1021/acsami.2c13392

[4] J. Ajayan et al., "Ferroelectric field effect transistors (FeFETs): Advancements, challenges and exciting prospects for next generation non-volatile memory (NVM) applications," *Mater. Today Commun.*, vol. 35, Jun. 2023, Art. no. 105591. https://www.sciencedirect.com/science/article/pii/S2352492823002817

[5] Q. Sun et al., "Total ionizing dose effects of 60Co γ-rays radiation on $Hf_xZr_{1-x}O_2$ ferroelectric thin film capacitors," *J. Mater. Sci., Mater. Electron.*, vol. 31, no. 3, pp. 2049–2056, Feb. 2020.

[6] C. C. Foster, "Total ionizing dose and displacement-damage effects in microelectronics," *MRS Bull.*, vol. 28, no. 2, pp. 136–140, Feb. 2003. [Online]. Available: https://www.cambridge.org/core/journals/mrs-bulletin/article/abs/total-ionizing-dose-and-displacementdamage-effects-in-microelectronics/234C117EF1017DAA91526546BD254126

[7] (Mar. 11, 2021). *Total Ionizing Dose Effects*. [Online]. Available: https://radhome.gsfc.nasa.gov/radhome/tid.htm

[8] J. Gasiot, "Radiation effects on devices: Total ionizing dose, displacement effect, single event effect," CERN Training; Available ATLAS Radiat. Hard Electron. Web Page, 2000.

[9] K.-Y. Chen, Y.-S. Tsai, and Y.-H. Wu, "Ionizing radiation effect on memory characteristics for HfO_2-based ferroelectric field-effect transistors," *IEEE Electron Device Lett.*, vol. 40, no. 9, pp. 1370–1373, Sep. 2019.

[10] S. Yan et al., "Modeling and simulation of ionizing radiation effect on ferroelectric field-effect transistor," *Jpn. J. Appl. Phys.*, vol. 55, no. 4, 2016, Art. no. 048001. [Online]. Available: https://iopscience.iop.org/article/10.7567/JJAP.55.048001

[11] Z. Jiang et al., "Evaluating the robustness of complementary channel ferroelectric FETs against total ionizing dose towards radiation-tolerant embedded nonvolatile memory," May 2023. [Online]. Available: https://www.techrxiv.org/articles/preprint/Evaluating_the_Robustness_of_Complementary_Channel_Ferroelectric_FETs_Against_Total_Ionizing_Dose_Towards_Radiation-Tolerant_Embedded_Nonvolatile_Memory/22933937, doi: 10.36227/techrxiv.22933937.v1.

[12] B. Trump, "Radiation handbook for electronics," Texas Instrum., Dallas, TX, USA, Tech. Rep., 2023.

[13] P. Fernández-Martínez, I. Cortés, S. Hidalgo, D. Flores, and F. R. Palomo, "Simulation of total ionising dose in MOS capacitors," in *Proc. 8th Spanish Conf. Electron Devices*, Feb. 2011, pp. 1–4.

[14] E. Yurchuk et al., "Charge-trapping phenomena in HfO_2-based FeFET-type nonvolatile memories," *IEEE Trans. Electron Devices*, vol. 63, no. 9, pp. 3501–3507, Sep. 2016.

[15] J. F. Salzman, "Total ionizing dose (TID) and single event effects (SEE) test report," Texas Instrum., Dallas, TX, USA, Tech. Rep. TPS7H1101-SP QMLV, Dec. 2013.

[16] T. R. Oldham and F. B. McLean, "Total ionizing dose effects in MOS oxides and devices," *IEEE Trans. Nucl. Sci.*, vol. 50, no. 3, pp. 483–499, Jun. 2003. [Online]. Available: https://ieeexplore.ieee.org/document/1208572/

[17] M. Poizat, "ESA Unclassified," Eur. Space Agency, Paris, France, Tech. Rep., 2016.

[18] Y. Huang et al., "TCAD simulation of total ionizing dose response on DSOI nMOSFET," in *Proc. Joint Int. EUROSOI Workshop Int. Conf. Ultimate Integr. Silicon (EUROSOI-ULIS)*, 2019, pp. 1–5.

[19] W. Zheng, K. H. Bowen, J. Li, I. Dąbkowska, and M. Gutowski, "Electronic structure differences in ZrO_2 vs HfO_2," *J. Phys. Chem. A*, vol. 109, no. 50, pp. 11521–11525, Dec. 2005, doi: 10.1021/jp053593e.

[20] A. K. Saha, M. Si, K. Ni, S. Datta, P. D. Ye, and S. K. Gupta, "Ferroelectric thickness dependent domain interactions in FEFETs for memory and logic: A phase-field model based analysis," in *IEDM Tech. Dig.*, Dec. 2020, p. 4.

[21] Synopsys, *Sentaurus Device Manual*.

[22] E. Chatzikyriakou, K. Potter, and C. H. de Groot, "A systematic method for simulating total ionizing dose effects using the finite elements method," *J. Comput. Electron.*, vol. 16, no. 3, pp. 548–555, Sep. 2017.

[23] R. C. Alig and S. Bloom, "Electron-hole-pair creation energies in semiconductors," *Phys. Rev. Lett.*, vol. 35, p. 1522, Dec. 1975. [Online]. Available: https://journals.aps.org/prl/abstract/10.1103/PhysRevLett.35.1522

[24] J.-L. Leray and P. Paillet, *Total Dose Effects: Modeling for Present and Future—1999 IEEE NSREC*. Ollainville, France: CEA/DAM Ile-de-France, IEEE Nuclear and Space Radiation Effects, Jul. 1999, p. 130.

[25] E. Chatzikyriakou, "Simulation of total ionizing dose and random dopant fluctuations in sub-100 nm transistor nodes," Ph.D. dissertation, Dept. Phys. Sci. Eng., School Electron. Comput. Sci., Univ. Southampton, Southampton, U.K., 2017.

[26] M. I. Khan and T. C. Upadhyay, "General introduction to ferroelectrics," in *Multifunctional Ferroelectric Materials*, D. R. Sahu, Ed. Rijeka: IntechOpen, 2021, ch. 2, doi: 10.5772/intechopen.97720.

[27] K. Toprasertpong, M. Takenaka, and S. Takagi, "Memory window in ferroelectric field-effect transistors: Analytical approach," *IEEE Trans. Electron Devices*, vol. 69, no. 12, pp. 7113–7119, Dec. 2022.

[28] J. Hoffman et al., "Ferroelectric field effect transistors for memory applications," *Adv. Mater*, vol. 22, nos. 26–27, pp. 2957–2961, Jul. 2010. [Online]. Available: https://onlinelibrary.wiley.com/doi/abs/10.1002/adma.200904327